Journal of Alloys and Compounds 509 (2011) 1157–1162

Contents lists available at ScienceDirect

Journal of Alloys and Compounds

journal homepage: www.elsevier.com/locate/jallcom

Influence of the ratio between Ni and $BaCe_{0.9}Y_{0.1}O_{3-\delta}$ on microstructural and electrical properties of proton conducting Ni–$BaCe_{0.9}Y_{0.1}O_{3-\delta}$ anodes

Milan Zunic[a,b,*], Laure Chevallier[c], Aleksandar Radojkovic[b], Goran Brankovic[b], Zorica Brankovic[b], Elisabetta Di Bartolomeo[a]

[a] Dipartimento di Scienze e Tecnologie Chimiche, Università di Roma "Tor Vergata", Via della Ricerca Scientifica 1, 00133 Rome, Italy
[b] Institute for Multidisciplinary Research, University of Belgrade, Kneza Viseslava 1, 11000 Belgrade, Serbia
[c] Institut Charles Gerhardt Montpellier, UMR 5253, Laboratoire des Agrégats, Interfaces et Matériaux pour l'Energie, Université Montpellier II, 34095 Montpellier cedex 5, France

ARTICLE INFO

Article history:
Received 23 March 2010
Received in revised form 31 August 2010
Accepted 1 September 2010
Available online 30 October 2010

Keywords:
Fuel cells
Anode
Cermet
Protonic conductor

ABSTRACT

Cermet anode substrates Ni–$BaCe_{0.9}Y_{0.1}O_{3-\delta}$ (Ni–BCY10) with varied ratios between Ni and BCY10 were prepared. BCY10 powders were prepared by the citrate–nitrate auto-combustion method and anode substrates were prepared by the method of evaporation and decomposition of solutions and suspensions. Sintered anode substrates were reduced and their properties were examined before and after reduction as a function of the ratio between Ni and BCY10. Microstructural properties of the pellets were investigated using X-ray diffraction analysis and field emission scanning electron microscopy. The influence of the Ni:BCY10 ratio on the microstructure of conducting paths through ceramic and metal parts was discussed. Impedance spectroscopy measurements were used for evaluation of electrical properties of the anode pellets. The high conductivity values of reduced anodes confirmed percolation through Ni particles even for an anode with a reduced amount of nickel. Fuel cell tests were carried out in order to examine the influence of the Ni:BCY10 ratio on fuel cell performance and to compare characteristics of cermet anodes with platinum electrodes. The ratio between Ni and BCY10 did have a slight influence on the power output of fuel cells. Fuel cells with a cermet anode demonstrated a higher power output compared to fuel cells with a platinum electrode.

1. Introduction

Application of composite anodes for the fabrication of intermediate temperature solid oxide fuel cells (IT-SOFCs) is one of the approaches used to reduce large anode overpotential caused by decreasing of the operating temperature. Composite anodes have a longer triple phase boundary (TPB) compared to anodes made of precious metals. In this kind of anodes electrochemical reactions are extended from the electrolyte/anode interface to the whole anode by creating an ion pathway. In the last decade this subject has been widely examined for commercial anodes based on oxide ion conductors (Ni–YSZ) [1–7]. Even if there are numerous literature data about this subject, electrochemical and microstructural properties of Ni–YSZ cermet anode are not completely investigated and still attract attention of researchers. Recently, Lee et al. investigated interconnection of NiO–YSZ cermet with stainless steel [8] and Zhang et al. studied impregnation of Sm-doped CeO_2 in Ni–YSZ anode [9]. Benyoucef et al. made cermet anodes of YSZ and different metals (Ni, Co and Cu) and investigate their thermal stability [10]. Jin et al. produce anode supported tubular SOFC using inverse method [11] and Wang et al. found that Cu–CeO_2 coating of Ni–YSZ can improve anode stability in H_2–CO syngas [12]. Li et al. investigated the effect of reduction temperature on the characteristics of anode-supported SOFC single cell [13] and Klemensø et al. were examined stability of Ni–YSZ abodes obtained by Ni impregnation using different sintering inhibitors [14].

By analogy with Ni–YSZ cermet anodes in contemporary SOFCs, the expected material of choice in the anode compartment of proton conducting fuel cells (PCFCs) is a cermet anode based on a metal, catalytically active to hydrogen, and a high temperature proton conductor (HTPC). Like in SOFCs based on oxide ion conductors, nickel cermets are usually used as anodes for PCFC as Ni expresses similar catalytic activity to precious metals, but offers significant cost savings [15,16]. Also, it has been reported that for HTPCs electrode materials are critical for power output and a Pt anode does not offer an acceptable performance [17–19]. The advantage of fuel cells utilizing a protonic conducting electrolyte is that they form water at the cathode, unlike SOFCs based on oxide ion conductors; hence the fuel at the anode remains pure thus eliminating the need for re-circulation.

* Corresponding author at: Department of Chemical Science and Technology, University of Rome Tor Vergata, Via della Ricerca Scientifica, 1, 00133 Rome, Italy. Tel.: +39 06 7259 4495; fax: +39 06 7259 4328.
E-mail address: milan.zunic@uniroma2.it (M. Zunic).

0925-8388/$ – see front matter © 2010 Elsevier B.V. All rights reserved.
doi:10.1016/j.jallcom.2010.09.144

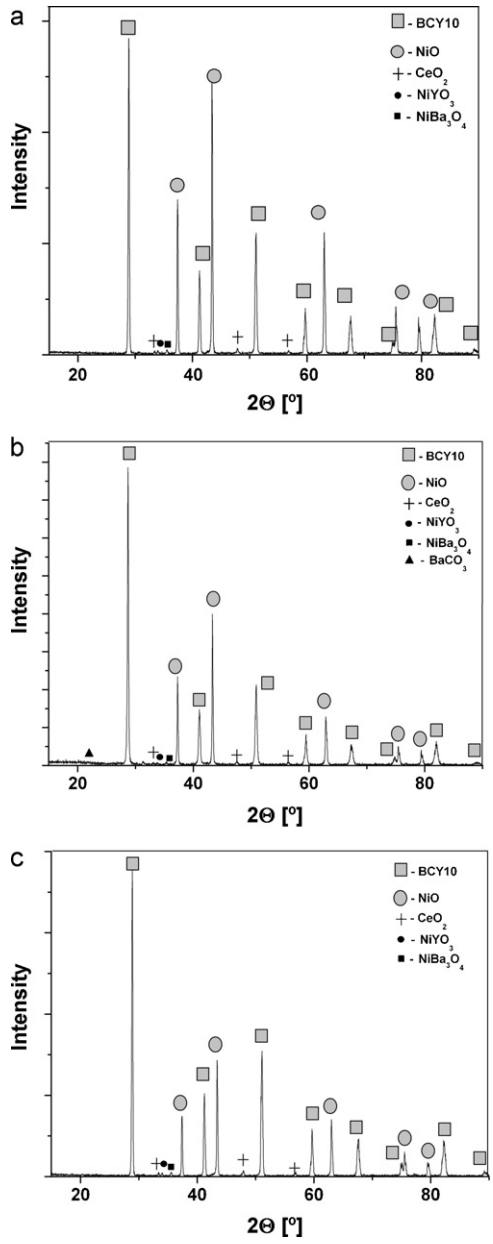

Fig. 1. XRD patterns of Anode 1(a), Anode 2 (b) and Anode 3 (c) sintered at 1400 °C for 5 h.

Even if this subject is very important for the performance of PCFC, only a few studies have been made of cermet anode materials based on HTPCs [20–28]. In addition, by our knowledge, only few methods have investigated preparation of Ni cermets based on HTPC: oxide powder mixture reaction [22] and the combustion method [29,30]. Recently, our group developed a wet-chemical route for the preparation of Ni–$BaCe_{0.9}Y_{0.1}O_{3-\delta}$ cermets [31]. That cermet material was successfully used for preparing anode substrates for electrophoretic deposition of a BCY10 electrolyte [32]. Fabrication of anode supported IT-SOFCs requires the use of anode substrates with a coefficient of thermal expansion (CTE) very close to CTE of the electrolyte. By decreasing the ratio between Ni and BCY10 in the anode composition, it is possible to avoid a thermal mismatch between the anode and electrolyte. A very important question is: how decreasing the ratio between Ni and BCY10 influences the performance of Ni–BCY10 anode substrates?

In this work anode substrates with different ratios between Ni and BCY10 were prepared. The influence of Ni:BCY10 ratio on the microstructural and electrical characteristics of anode substrates was investigated before and after reduction. Fuel cell tests were performed to observe fuel cell performance as a function of the Ni:BCY10 ratio and to compare the characteristics of cermets with platinum anodes.

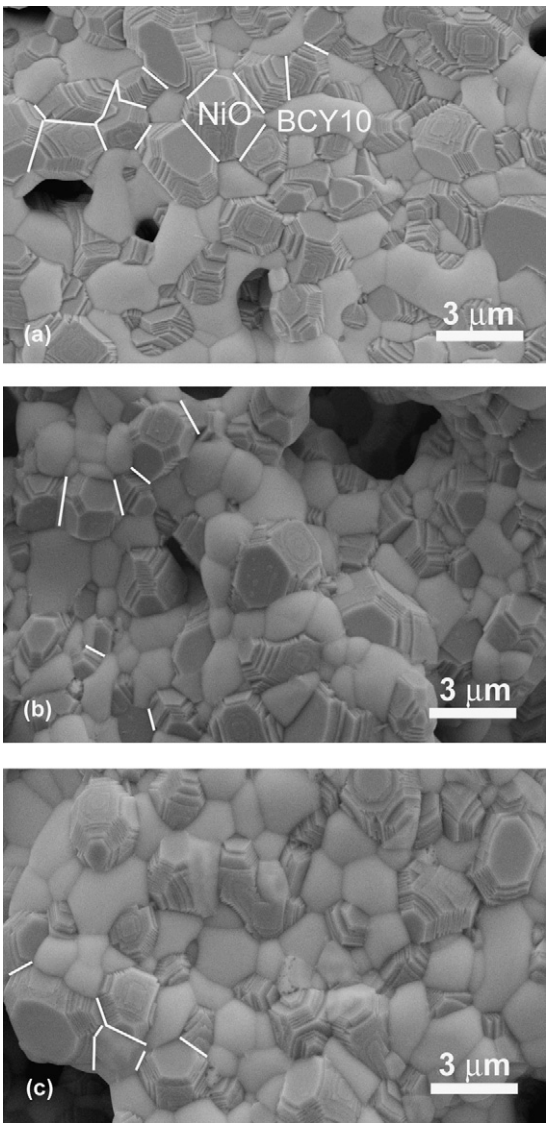

Fig. 2. SEM micrographs of (a) Anode 1, (b) Anode 2 and (c) Anode 3 sintered at 1400 °C for 5 h.

2. Experimental

The protonic conductor material was prepared by the citrate–nitrate auto-combustion method using $Ba(NO_3)_2$ (Aldrich, 99.999%), $Ce(NO_3)_2{\cdot}6H_2O$ (Aldrich, 99.999%) and $Y(NO_3)_2{\cdot}6H_2O$ (Aldrich, 99.9%) as starting reactants and citric acid as the combustion fuel. This synthesis has been described in detail elsewhere [33]. The obtained powder was fired at 1000 °C for 10 h and characterized by X-ray diffraction (XRD, Philips X'pert D500) analysis and field emission scanning electron microscopy (FE-SEM, Leo Supra 1250).

In order to obtain uniform distribution of NiO grains in the BCY10 ceramic, NiO–BCY10 cermet composite powders were prepared using a wet-chemical route [31]. The starting reactants were $Ni(NO_3)_2{\cdot}6H_2O$ (Aldrich, 99.99%) and already prepared BCY10. The weight ratios between Ni and BCY10 were 60:40, 50:50 and 40:60. The resulting powders were milled in an agate mortar and calcined at 1000 °C for 5 h.

The anode slurry was prepared mixing polyvinyl alcohol (PVA, Aldrich, 99.9%), NiO–BCY10 cermet powders and graphite powder (<20 μm, Aldrich) in water. The graphite powder has the role of pore former and PVA has the role of binder. The weight ratio between cermet, graphite, and PVA was 70:25:5, respectively. Cylindrical anode pellets with a diameter of 13 mm and a thickness of about 0.7 mm

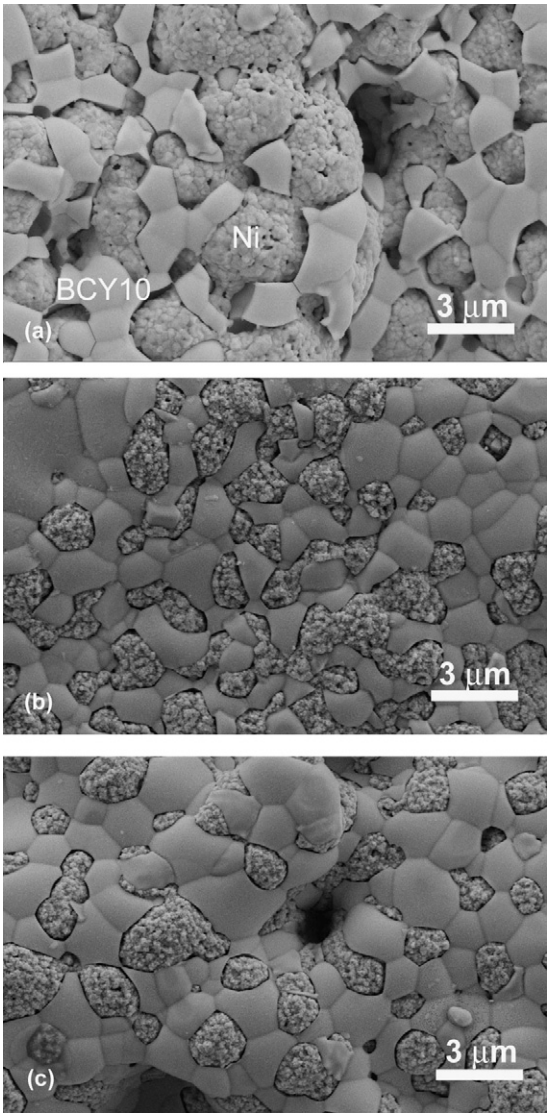

Fig. 3. SEM micrographs of (a) Anode 1, (b) Anode 2 and (c) Anode 3 sintered at 1400 °C for 5 h after reduction treatment.

were uniaxially pressed at 150 MPa and sintered at 1400 °C for 5 h. Anode substrates before reduction were marked as follows: Anode 1 (Ni:BCY10 = 60:40), Anode 2 (Ni:BCY10 = 50:50) and Anode 3 (Ni:BCY10 = 40:60). After reduction anode substrates are marked as follows: A1 (Ni:BCY10 = 60:40), A2 (Ni:BCY10 = 50:50) and A3 (Ni:BCY10 = 40:60). The expected volume ratio Ni:BCY10 in A1 is 55:45, in A2 is 45:55 and in A3 is 36:64.

Electrochemical impedance spectroscopy (EIS) measurements of anode pellets were performed in the range of temperatures from 550 to 700 °C and in the range of frequencies from 0.1 Hz to 1 MHz with the AC voltage amplitude of 50 mV before and

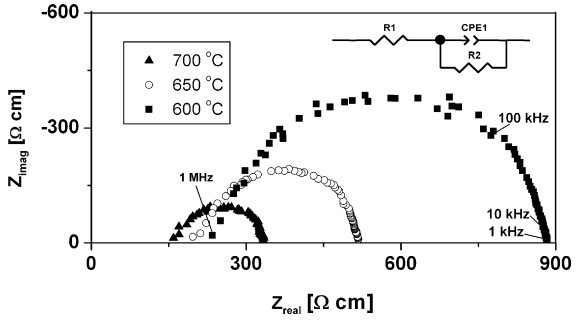

Fig. 4. Nyquist plot of Anode 1 in Ar atmosphere measured before reduction.

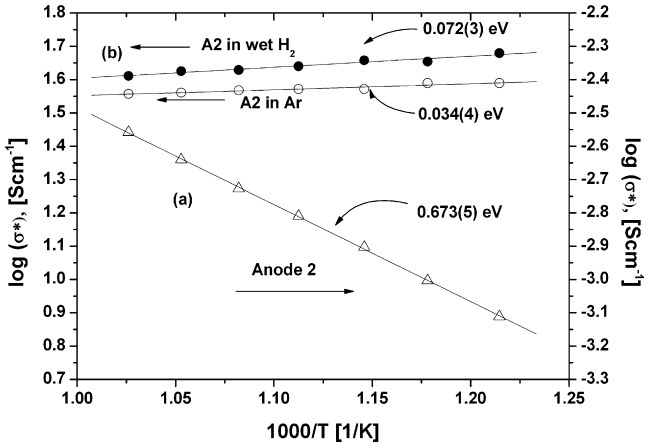

Fig. 5. Arrhenius plots of the Anode 2 pellet in Ar atmosphere before reduction treatment (a) and A2 pellet both in Ar and in wet H_2 gas mixture after reduction treatment.

after reduction in wet H_2. The impedance plots were fitted by ZView® for Windows software (Version 2.8).

Hydrogen–air fuel cell experiments were carried out in the range of temperatures from 600 to 750 °C. BCY10 powder was uniaxially pressed at 150 MPa and sintered at 1550 °C for 5 h. Commercial printing oil and NiO–BCY10 anode powders were mixed together to form a slurry, which was brush painted on a dense BCY10 pellet and then fired at 1400 °C for 5 h. $La_{0.8}Sr_{0.2}Co_{0.8}Fe_{0.2}O_3$ (LSCF)–$BaCe_{0.9}Yb_{0.1}O_{3-\delta}$ (10YbBC) composite cathode powders mixed with commercial printing oil were tape cast on a BCY10 dense pellet and then fired at 1100 °C for 2 h. These composite cathode powders were specifically optimized for a BCY proton conductor electrolyte [34]. The diameter of electrode active area was 7 mm (A = 0.384 cm^2) and the diameter of the electrolyte pellet after sintering was 9.85 mm. The cathode thickness was 80 ± 5 μm. Gold wires were fixed with a drop of platinum paste (Engelhard-Clal) on the top of the anode and cathode and used as current collectors. For the fuel cell tests, samples were mounted at the end of an alumina tube using a gas tight ceramic paste seal (Aremco, 552). The anode was exposed to wet hydrogen (3 vol.% H_2O) while the cathode was exposed to ambient air. Electrochemical measurements were performed using a multichannel potentiostat VMP3 (Princeton Applied Research). The cell was equilibrated at open-circuit for about 10 min before EIS measurements.

3. Results and discussion

In Fig. 1(a)–(c) XRDs patterns of Anode 1, Anode 2 and Anode 3 are shown, respectively. All graphs show the presence of two phases according to reference patterns JCPDS 78-0643 for NiO and JCPDS 82-2372 for BCY. Also, traces of $BaCO_3$ (JCPDS 71-2394) and CeO_2 (JCPDS 65-2975) are detected (with relative intensity less than 2%). Appearance of $BaCO_3$ and CeO_2 peaks could be the result of insta-

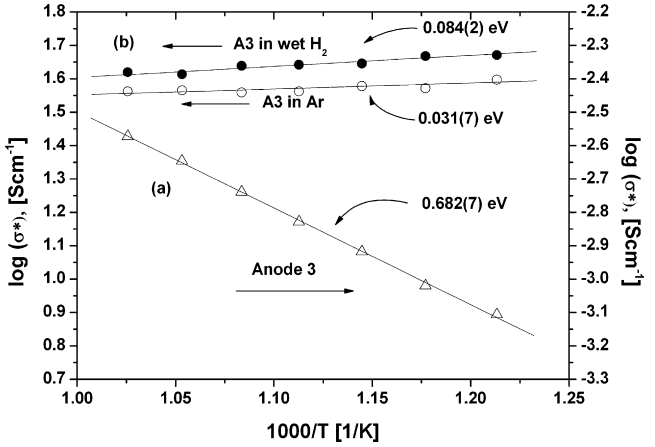

Fig. 6. Arrhenius plots of the Anode 3 pellet in Ar atmosphere before reduction treatment (a) and A3 pellet both in Ar and in wet H_2 gas mixture after reduction treatment.

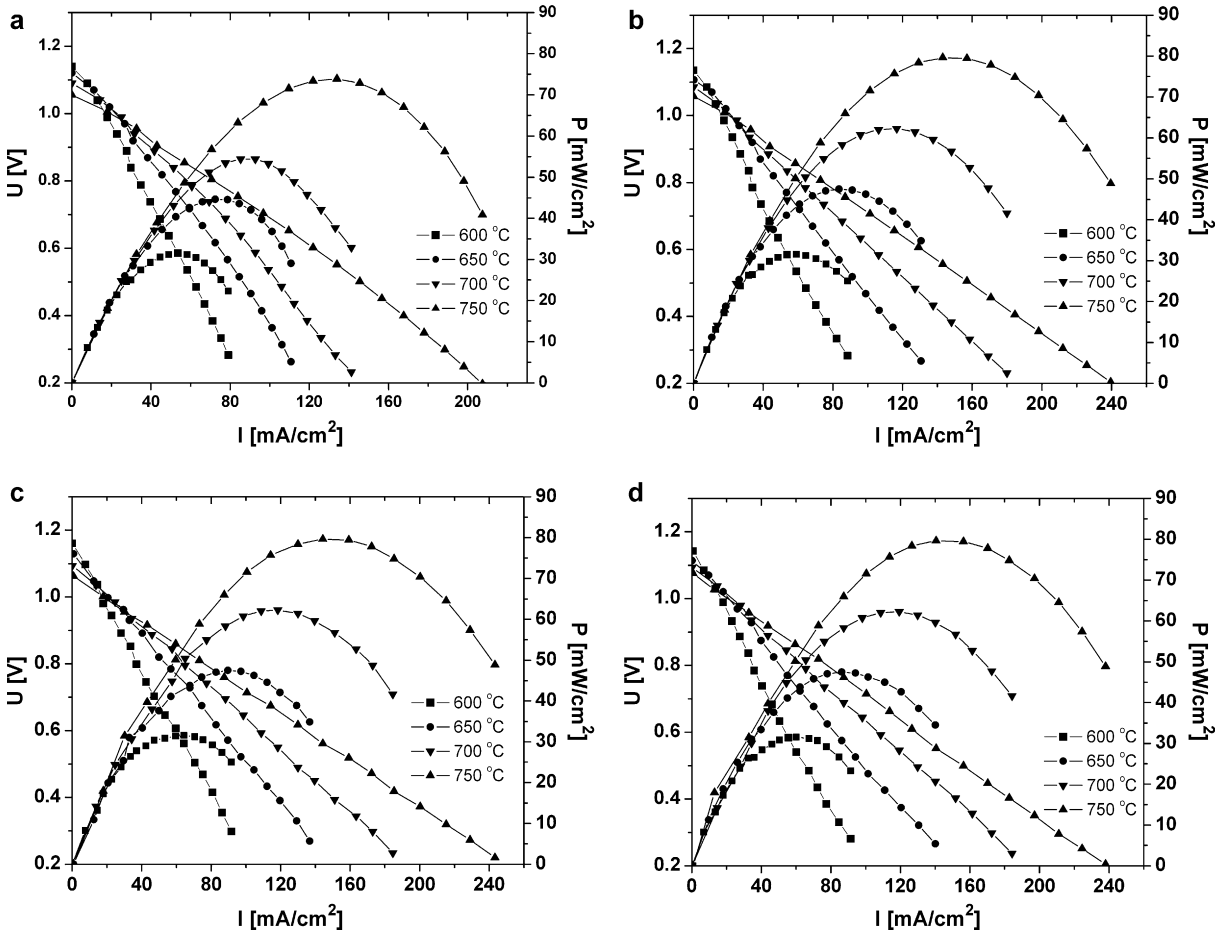

Fig. 7. *I–V* curves and power outputs of: (a) Pt/BCY10/LSCF-10YbBC, (b) Anode 1/BCY10/LSCF-10YbBC, (c) Anode 2/BCY10/LSCF-10YbBC and (d) Anode 3/BCY10/LSCF-10YbBC.

bility of the BCY10 powder in CO_2 atmosphere [35] or it could be result of precursor excess. XRD analysis also detected the presence of $Y(NiO_3)$ (JCPDS 89-9057) and $NiBa_3O_4$ (JCPDS 85-0907) phases which are the result of a reaction between Ni and elements in the electrolyte. After reduction Anode 1, Anode 2 and Anode 3 in wet H_2, NiO reduced to Ni and XRD analysis showed the presence of a Ni phase and a BCY10 orthorhombic phase.

For proper anode functionality, it is very important to obtain a uniform distribution of its components in the microstructure. Compared to metals with a high catalytic activity, composite cermet anodes have a triple phase boundary extended to the whole anode volume. To provide proper catalytic functionality of cermet anodes the microstructure should consist of two continuous components: ceramics and Ni sublattice. SEM micrographs of Anode 1, Anode 2 and Anode 3 are shown in Fig. 2(a)–(c), respectively. All compositions have similar microstructures with good distribution of NiO and BCY10 grains and grain sizes of both phases below 3 μm. The only visible difference among these three compositions is the longitude of the grain boundary between NiO grains and between BCY10 grains. Some grain boundaries between NiO grains are marked with a white line in Fig. 2. As expected, this longitude decreases with decreasing of the Ni amount. The consequence of this barely visible difference between anode microstructures could result in different thermal expansion coefficients between microstructures and could have an influence on the electrical properties of anodes and on the performance of fuel cells that use these anodes.

This difference in microstructure is more visible after the reduction of anodes. In Fig. 3 SEM micrographs of anodes after reduction are shown. The well-defined grain boundaries between NiO grains that were observable before reduction still exist between Ni grains, but they are less evident. Instead of NiO grains before reduction, big Ni aggregates formed and connected together after reduction. In the microstructure of A1 (Fig. 3(a)) Ni dominates, the sublattice of Ni is continual and the grains of BCY10 are not continuously connected in the whole anode volume. With decreasing amount of Ni, the sublattice of BCY10 is more continual, as shown in Fig. 3(b) for A2. Anode A3, which contains the smallest amount of Ni, among the three studied samples, has completely connected BCY10 grains.

To examine the influence of different microstructures on the electrical characteristics of anodes, EIS measurements were performed. As an example, EIS plots of Anode 1 before reduction at different temperatures and an equivalent circuit are shown in Fig. 4. Similar plots with slightly depressed semicircles were obtained also for Anode 2 and Anode 3. The contribution of NiO and BCY10 could not be resolved from impedance spectra. The total resistance of the sample determined from the impedance spectra is the sum of $R_{total} = R_b + R_{gb}$, where R_b is the bulk resistance and R_{gb} is the grain boundary resistance. The total resistance of a sample depends on the resistance of the grain boundary, which decreases with sample densification. In the range of intermediate temperatures, semicircles arising from bulk and grain boundary resistances cannot be resolved [36]. Chiodelli et al. [37] showed that the contribution of grain boundary resistance in BCY10 is visible at lower temperatures (around 200 °C) and they also found that the impedance of a grain boundary could be 10 times higher compared to impedance of the bulk when the density of the sample is low.

Figs. 5 and 6 show Arrhenius plots extracted from the values of total resistances in EIS measurements for the pellets Anode 2 and

Table 1
Values of OCV and power density output for samples tested at different temperatures.

Samples	OCV [V]				P [mW/cm^2]			
	600 °C	650 °C	700 °C	750 °C	600 °C	650 °C	700 °C	750 °C
Pt/BCY10/LSCF-10YbBC	1.13	1.12	1.09	1.05	31	45	54	74
Anode 1/BCY10/LSCF-10YbBC	1.13	1.11	1.05	1.04	32	47	63	80
Anode 2/BCY10/LSCF-10YbBC	1.15	1.12	1.09	1.06	31	46	62	79
Anode 3/BCY10/LSCF-10YbBC	1.14	1.11	1.09	1.07	30	46	60	78

Anode 3, respectively, in Ar atmosphere before reduction treatment (a) and of reduced anode pellets A2 and A3, respectively, both in Ar and in wet H_2 gas mixtures (b). Compared to the Arrhenius plot of Anode 1 [31], the values of activation energies are slightly different. As in the case of Anode 1, EIS of Anode 2 and Anode 3 pellets showed a single depressed semicircle. The activation energies for both samples before reduction are around 0.7 eV, which was attributed to the BCY10 component in the anode pellets. Also in the case of reduced anodes, the EIS plots showed a merely resistive behavior, indicating metallic conductivity. Negative slopes in the Arrhenius plots confirmed that metallic conduction took place for the reduced pellets both in Ar and in wet H_2 gas mixtures. As in the A1 sample, the high conductivity values, above 40 S cm^{-1}, confirmed that percolation through Ni particles took place properly in samples A2 and A3, even though the amount of Ni is decreased.

In order to compare performances of Anode 1, Anode 2 and Anode 3 with performances of Pt, four cells were made: Pt/BCY10/LSCF-10YbBC, Anode 1/BCY10/LSCF-10YbBC, Anode 2/BCY10 /LSCF-10YbBC and Anode 3/BCY10 /LSCF-10YbBC. Fig. 7 shows *I–V* curves and power density output of these four cells obtained exposing the anode to wet H_2 and the cathode to ambient air in the range of temperatures from 600 to 750 °C. All samples have open circuit voltage (OCV) close to the theoretical value (1.17 V at 600 °C). The cell with Anode 1 has the highest maximum power density of 80 mW/cm^2 at the temperature of 750 °C. All measurement results are summarized in Table 1.

Fig. 8 shows a maximum power density comparison of a single cell with different anodes at different temperatures. Since the material compositions and preparation conditions for the electrolyte and cathode, as well as the cell fabrication steps, were identical for all single cells, it can be concluded that the performance difference of these cells is caused by the anode properties. The difference between fuel cells with cermet anodes and ones with a Pt anode is very small at temperatures of 600 and 650 °C, but at 700 and 750 °C the maximum power output of the fuel cell with a Pt anode decreases. All cells with cermet anodes have better performances compared to cells with Pt as an anode. This could be explained by the fact that in a Pt anode electrochemical reactions occur at the triple phase boundary that exists only at the electrolyte/anode interface. On the other hand, in cells with cermet anodes these reactions are extended to the whole anode volume. The differences between maximum power densities of cells with cermet anodes are small, but in the whole range of temperatures it is possible to observe a slight reduction of the maximum power output with decrease of the Ni amount.

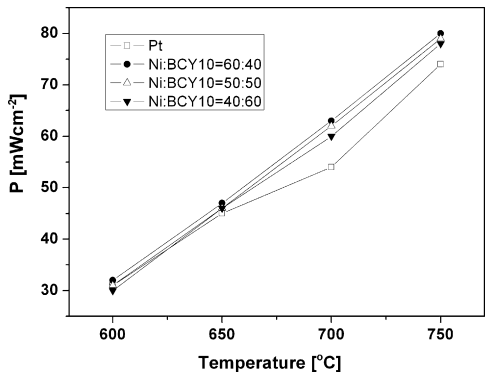

Fig. 8. Performance comparison of a single cell with different anode types at different temperatures.

4. Conclusions

Anode substrates with different ratios of Ni and BCY10 were synthesized without the presence of secondary phases. A homogeneous distribution of composite phases in the microstructure was obtained. Decreasing of the Ni:BCY10 ratio has a considerable influence on the microstructure of conducting pathways in anode substrates, but electrical characterization showed comparable activation energies of samples before and after reduction. High conductivity values ($\sigma^* > 40$ S cm^{-1}) of all samples after reduction confirmed that percolation through Ni particles took place properly even though the amount of Ni decreased. Fuel cell tests showed very small reduction (less than 5%) in the maximum power output between fuel cells with the highest and the lowest amount of nickel in the anode composition. The conclusion is that an anode with 40 wt.% of nickel could be used for fabrication of anode supported PCFC without any significant performance deterioration. Fuel cells with composite anode substrates showed a higher maximum power output compared to a fuel cell with a platinum anode.

Acknowledgements

This work has been funded by the Ministry of University and Research (MiUR) of Italy under the frame of the FISR project "Polymeric and Ceramic Fuel Cells: System Validation and Development of New Materials" and of the PRIN project "Protonic Conducting Ceramics for Fuel Cells" and by the Ministry of Science and Technology Development of the Republic of Serbia (project number OI 142040).

References

[1] W. Bao, H. Guan, J. Cheng, J. Power Sources 175 (2008) 232.
[2] C. Sun, U. Stimming, J. Power Sources 171 (2007) 247.
[3] Q. Fu, F. Tietz, D. Sebold, S. Tao, J.T.S. Irvine, J. Power Sources 171 (2007) 663.
[4] N. Ai, Z. Lu, K. Chen, X. Huang, X. Du, W. Su, J. Power Sources 171 (2007) 489.
[5] S.D. Kim, J.J. Lee, H. Moon, S.H. Hyun, J. Moon, J. Kim, H.W. Lee, J. Power Sources 169 (2007) 265.
[6] S.D. Kim, H. Moon, S.H. Hyun, J. Moon, J. Kim, H.W. Lee, J. Power Sources 163 (2006) 392.
[7] H. Li, C. Xia, Z. Zhou, M. Zhu, G. Meng, J. Mater. Sci. 41 (2006) 3185.
[8] S. Lee, K.-H. Kang, H.S. Hong, Y. Yun, J.-H. Ahn, J. Alloys Compd. 488 (2009) L1.
[9] L. Zhang, J. Gao, M. Liu, C. Xia, J. Alloys Compd. 482 (2009) 168.
[10] A. Benyoucef, D. Klein, O. Rapaud, C. Coddet, B. Benyoucef, J. Phys. Chem. Solids 70 (2009) 1487.
[11] C. Jin, J. Liu, L. Li, Y. Bai, J. Membr. Sci. 341 (2009) 233.
[12] X.-F. Ye, S.R. Wang, J. Zhou, F.R. Zeng, H.W. Nie, T.L. Wen, J. Power Sources 195 (2010) 7264.
[13] T.S. Li, W.G. Wang, H. Miao, T. Chen, C. Xu, J. Alloys Compd. 495 (2010) 138.
[14] T. Klemensø, K. Thydén, M. Chen, H.-J. Wang, J. Power Sources 195 (2010) 7295.
[15] H. Iwahara, H. Uchida, S. Tanaka, Solid State Ionics 9&10 (1983) 1021.
[16] Y. Matsuzaki, I. Yasuda, Solid State Ionics 152–153 (2002) 463.
[17] J.M. Serra, W.A. Meulenberg, J. Am. Ceram. Soc. 90 (2007) 2082.

[18] E. Fabbri, A. D'Epifanio, E. Di Bartolomeo, S. Licoccia, E. Traversa, Solid State Ionics 179 (2008) 558.
[19] E. Fabbri, D. Pergolesi, A. D'Epifanio, E. Di Bartolomeo, G. Balestrino, S. Licoccia, E. Traversa, Energy Environ. Sci. 1 (2008) 355.
[20] P. Ranran, W. Yan, Y. Lizhai, M. Zongqiang, Solid State Ionics 177 (2006) 389.
[21] N. Maffei, L. Pelletier, A. McFarlan, J. Power Sources 136 (2004) 24.
[22] T.H. Lee, S.E. Dorris, U. Balachandran, Solid State Ionics 176 (2005) 1479.
[23] J. Le, L.N. van Rij, J. Schoonman, J. Electrochem. Soc. 147 (2000) 4345.
[24] L.N. Van Rij, J. Le, R.C. Van Landschoot, J. Schoonman, J. Mater. Sci. 36 (2001) 1069.
[25] V. Agarwal, M. Liu, J. Electrochem. Soc. 144 (1997) 1035.
[26] G.C. Mather, D.P. Fagg, A. Ringuedé, J.R. Frade, Fuel Cells 1 (2001) 233.
[27] M.L. Fontaine, Y. Larring, R. Haugsrud, T. Norby, K. Wiik, R. Bredesen, J. Power Sources 188 (2009) 106.
[28] L. Yan, W. Sun, L. Bi, S. Fang, Z. Tao, W. Liu, J. Alloys Compd. (2010), doi:10.1016/j.jallcom.2010.08.040.
[29] G.C. Mather, F.M. Figueiredo, D.P. Fagg, T. Norby, J.R. Jurado, J.R. Frade, Solid State Ionics 158 (2003) 333.
[30] A. Essoumhi, G. Taillades, M. Taillades-Jacquin, D.J. Jones, J. Rozière, Solid State Ionics 179 (2008) 2155.
[31] L. Chevallier, M. Zunic, V. Esposito, E. Di Bartolomeo, E. Traversa, Solid State Ionics 180 (2009) 715.
[32] M. Zunic, L. Chevallier, F. Deganello, A. D'Epifanio, S. Licoccia, E. Di Bartolomeo, E. Traversa, J. Power Sources 190 (2009) 417.
[33] F. Deganello, G. Marcì, G. Deganello, J. Eur. Ceram. Soc. 29 (2009) 439.
[34] E. Fabbri, S. Licoccia, E. Traversa, E.D. Wachsman, Fuel Cells 2 (2009) 128.
[35] N. Zakowsky, S. Williamson, J.T.S. Irwine, Solid State Ionics 176 (2005) 3019.
[36] Z. Khani, M. Taillades-Jacquin, G. Taillades, M. Marrony, D.J. Jones, J. Roziere, J. Solid State Chem. 182 (2009) 790.
[37] G. Chiodelli, L. Malavasi, C. Tealdi, S. Barison, M. Battagliarin, L. Doubova, M. Fabrizio, C. Mortalò, R. Gerbasi, J. Alloys Compd. 470 (2009) 477.